Year: 2018

Photon Counting Computed Tomography With Dedicated Sharp Convolution Kernels: Tapping the Potential of a New Technology for Stent Imaging

von Spiczak, Jochen ; Mannil, Manoj ; Peters, Benjamin ; Hickethier, Tilman ; Baer, Matthias ; Henning, André ; Schmidt, Bernhard ; Flohr, Thomas ; Manka, Robert ; Maintz, David ; Alkadhi, Hatem

Abstract: OBJECTIVES The aims of this study were to assess the value of a dedicated sharp convolution kernel for photon counting detector (PCD) computed tomography (CT) for coronary stent imaging and to evaluate to which extent iterative reconstructions can compensate for potential increases in image noise. MATERIALS AND METHODS For this in vitro study, a phantom simulating coronary artery stenting was prepared. Eighteen different coronary stents were expanded in plastic tubes of 3 mm diameter. Tubes were filled with diluted contrast agent, sealed, and immersed in oil calibrated to an attenuation of -100 HU simulating epicardial fat. The phantom was scanned in a modified second generation 128-slice dual-source CT scanner (SOMATOM Definition Flash, Siemens Healthcare, Erlangen, Germany) equipped with both a conventional energy integrating detector and PCD. Image data were acquired using the PCD part of the scanner with 48 × 0.25 mm slices, a tube voltage of 100 kVp, and tube current-time product of 100 mAs. Images were reconstructed using a conventional convolution kernel for stent imaging with filtered back-projection (B46) and with sinogram-affirmed iterative reconstruction (SAFIRE) at level 3 (I463). For comparison, a dedicated sharp convolution kernel with filtered back-projection (D70) and SAFIRE level 3 (Q703) and level 5 (Q705) was used. The D70 and Q70 kernels were specifically designed for coronary stent imaging with PCD CT by optimizing the image modulation transfer function and the separation of contrast edges. Two independent, blinded readers evaluated subjective image quality (Likert scale 0-3, where 3 = excellent), in-stent diameter difference, in-stent attenuation difference, mathematically defined image sharpness, and noise of each reconstruction. Interreader reliability was calculated using Goodman and Kruskal's and intraclass correlation coefficients (ICCs). Differences in image quality were evaluated using a Wilcoxon signed-rank test. Differences in in-stent diameter difference, in-stent attenuation difference, image sharpness, and image noise were tested using a paired-sample t test corrected for multiple comparisons. RESULTS Interreader and intrareader reliability were excellent (= 0.953, ICCs = 0.891-0.999, and = 0.996, ICCs = 0.918-0.999, respectively). Reconstructions using the dedicated sharp convolution kernel yielded significantly better results regarding image quality (B46: 0.4 ± 0.5 vs D70: 2.9 ± 0.3; $P < 0.001$), in-stent diameter difference (1.5 ± 0.3 vs 1.0 ± 0.3 mm; $P < 0.001$), and image sharpness (728 ± 246 vs 2069 ± 411 CT numbers/voxel; $P < 0.001$). Regarding in-stent attenuation difference, no significant difference was observed between the 2 kernels (151 ± 76 vs 158 ± 92 CT numbers; $P = 0.627$). Noise was significantly higher in all sharp convolution kernel images but was reduced by 41% and 59% by applying SAFIRE levels 3 and 5, respectively (B46: 16 ± 1, D70: 111 ± 3, Q703: 65 ± 2, Q705: 46 ± 2 CT numbers; $P < 0.001$ for all comparisons). CONCLUSIONS A dedicated sharp convolution kernel for PCD CT imaging of coronary stents yields superior qualitative and quantitative image characteristics compared with conventional reconstruction kernels. Resulting higher noise levels in sharp kernel PCD imaging can be partially compensated with iterative image reconstruction techniques.

DOI: https://doi.org/10.1097/RLI.0000000000000485

Originally published at:
von Spiczak, Jochen; Mannil, Manoj; Peters, Benjamin; Hickethier, Tilman; Baer, Matthias; Henning, André; Schmidt, Bernhard; Flohr, Thomas; Manka, Robert; Maintz, David; Alkadhi, Hatem (2018). Photon Counting Computed Tomography With Dedicated Sharp Convolution Kernels: Tapping the Potential of a New Technology for Stent Imaging. Investigative Radiology, 53(8):486-494.
DOI: https://doi.org/10.1097/RLI.0000000000000485

Photon Counting Computed Tomography With Dedicated Sharp Convolution Kernels

Tapping the Potential of a New Technology for Stent Imaging

Jochen von Spiczak, MD, MSc, Manoj Mannil, MD, MSc,* Benjamin Peters, MD,* Tilman Hickethier, MD,† Matthias Baer, PhD,‡ André Henning, MSc, MSc,‡ Bernhard Schmidt, PhD,‡§ Thomas Flohr, PhD,‡ Robert Manka, MD,*||¶ David Maintz, MD,† and Hatem Alkadhi, MD, MPH, EBCR**

Objectives: The aims of this study were to assess the value of a dedicated sharp convolution kernel for photon counting detector (PCD) computed tomography (CT) for coronary stent imaging and to evaluate to which extent iterative reconstructions can compensate for potential increases in image noise.

Materials and Methods: For this in vitro study, a phantom simulating coronary artery stenting was prepared. Eighteen different coronary stents were expanded in plastic tubes of 3 mm diameter. Tubes were filled with diluted contrast agent, sealed, and immersed in oil calibrated to an attenuation of −100 HU simulating epicardial fat. The phantom was scanned in a modified second generation 128-slice dual-source CT scanner (SOMATOM Definition Flash, Siemens Healthcare, Erlangen, Germany) equipped with both a conventional energy integrating detector and PCD. Image data were acquired using the PCD part of the scanner with 48 × 0.25 mm slices, a tube voltage of 100 kVp, and tube current-time product of 100 mAs. Images were reconstructed using a conventional convolution kernel for stent imaging with filtered back-projection (B46) and with sinogram-affirmed iterative reconstruction (SAFIRE) at level 3 ($I46_3$). For comparison, a dedicated sharp convolution kernel with filtered back-projection (D70) and SAFIRE level 3 ($Q70_3$) and level 5 ($Q70_5$) was used. The D70 and Q70 kernels were specifically designed for coronary stent imaging with PCD CT by optimizing the image modulation transfer function and the separation of contrast edges. Two independent, blinded readers evaluated subjective image quality (Likert scale 0–3, where 3 = excellent), in-stent diameter difference, in-stent attenuation difference, mathematically defined image sharpness, and noise of each reconstruction. Interreader reliability was calculated using Goodman and Kruskal's γ and intraclass correlation coefficients (ICCs). Differences in image quality were evaluated using a Wilcoxon signed-rank test. Differences in in-stent diameter difference, in-stent attenuation difference, image sharpness, and image noise were tested using a paired-sample *t* test corrected for multiple comparisons.

Results: Interreader and intrareader reliability were excellent ($\gamma = 0.953$, ICCs = 0.891–0.999, and $\gamma = 0.996$, ICCs = 0.918–0.999, respectively). Reconstructions using the dedicated sharp convolution kernel yielded significantly better results regarding image quality (B46: 0.4 ± 0.5 vs D70: 2.9 ± 0.3; $P < 0.001$), in-stent diameter difference (1.5 ± 0.3 vs 1.0 ± 0.3 mm; $P < 0.001$), and image sharpness (728 ± 246 vs 2069 ± 411 CT numbers/voxel; $P < 0.001$). Regarding in-stent attenuation difference, no significant difference was observed between the 2 kernels (151 ± 76 vs 158 ± 92 CT numbers; $P = 0.627$). Noise was significantly higher in all sharp convolution kernel images but was reduced by 41% and 59% by applying SAFIRE levels 3 and 5, respectively (B46: 16 ± 1, D70: 111 ± 3, $Q70_3$: 65 ± 2, $Q70_5$: 46 ± 2 CT numbers; $P < 0.001$ for all comparisons).

Conclusions: A dedicated sharp convolution kernel for PCD CT imaging of coronary stents yields superior qualitative and quantitative image characteristics compared with conventional reconstruction kernels. Resulting higher noise levels in sharp kernel PCD imaging can be partially compensated with iterative image reconstruction techniques.

Key Words: computed tomography, photon counting detector, coronary artery stents, convolution kernel

(*Invest Radiol* 2018;00: 00–00)

Noninvasive coronary artery stent imaging remains a major challenge, despite the considerable improvements in imaging technologies in the past years. The technique currently showing most promise for coronary artery stent imaging is computed tomography (CT), which has become a clinically relevant modality for imaging of native coronary arteries and bypass grafts.[1,2] Coronary artery stent imaging with CT, however, remains to have shortcomings[3] because the stent material causes blooming, beam hardening, and photon starvation.[4]

Photon counting detector (PCD) technology has been recently introduced for CT imaging,[5–8] and clinical feasibility of the new technology has been shown.[6] While conventional energy integrating detectors (EIDs) convert incoming photons into electric currents indirectly using intermediate scintillator and photodiode layers, PCDs directly convert x-ray photons into proportional electric signals using semiconductor materials like cadmium telluride (CdTe). The semiconductor layer is enclosed by a planar cathode on the top and a grid of pixelated anodes on the bottom with a high voltage applied in between (bias voltage). When an x-ray photon hits the detector, a cloud of free electric charges proportional to the energy of the incident photon is induced. The electric field transports the free charge particles to the anode pixels, in which an electric current is induced. Fast read-out electronics (including pulse shaping, pulse height discriminators, and counters) count each generated electronic pulse with a duration of a few nanoseconds.

These technical characteristics of PCDs offer various advantages over conventional EID technology. First, higher spatial resolution can be achieved because of smaller PCD detector pixels. Other than for conventional EIDs, no optically intransparent separators blocking optical photons between adjacent detector elements are needed, since the incoming photon flux is directly converted into an electric signal. Ultra-high resolution (so-called "SHARP" mode) with an effective detector size of 0.25 × 0.25 mm at the isocenter becomes possible, compared to 0.5 × 0.5 mm of the standard PCD "MACRO" mode and 0.5 to 0.625 mm of commercial EIDs.[9] Second, higher dose efficiency is possible applying PCD technology. In EIDs, x-ray photons hitting the

Received for publication January 11, 2018; and accepted for publication, after revision, March 30, 2018.

From the *Institute of Diagnostic and Interventional Radiology, University Hospital Zurich, Switzerland; †Department of Radiology, University Hospital of Cologne; ‡Siemens Healthcare GmbH, Forchheim; §Institute of Medical Physics, University Erlangen-Nuremberg, Erlangen, Germany; ||Department of Cardiology, University Heart Center, University Hospital Zurich; and ¶Institute for Biomedical Engineering, University and ETH Zurich, Switzerland.

Conflicts of interest and sources of funding: none declared.

Supplemental digital contents are available for this article. Direct URL citations appear in the printed text and are provided in the HTML and PDF versions of this article on the journal's Web site (www.investigativeradiology.com).

Correspondence to: Hatem Alkadhi, MD, MPH, EBCR, Institute of Diagnostic and Interventional Radiology, University Hospital Zurich, Raemistrasse 100, 8091 Zurich, Switzerland. E-mail: hatem.alkadhi@usz.ch.

ISSN: 0020-9996/18/0000–0000
DOI: 10.1097/RLI.0000000000000485

optical separation layers do not contribute to the measured signal and decrease the dose efficiency. Because these blocking areas do not scale with the pixel size, the dose inefficiency of EIDs even increases with smaller pixel size, whereas in PCDs, no such separators are needed. Third, PCDs offer inherent spectral capabilities because of the direct conversion of x-ray photons into proportional electric currents, which can be used for iodine concentration measurements[10] and material decomposition analysis.[11–13] It is common practice to define certain energy ranges (so-called "energy bins") that registered photons with similar energies are categorized in.[14] Fourth, without the intermediate transformation step needed in EIDs, the electronic noise of PCDs is lower, translating into lower image noise and higher contrast-to-noise ratios.[6,15,16]

In theory, such technical advances of PCD arrays should translate into an improved image quality and better coronary stent evaluation. In a first in vitro study, Mannil et al[17] found increased overall image quality, improved in-stent lumen delineation, and reduced blooming artifacts. However, the authors of that study[17] compared data sets acquired with identical settings between PCD and EID and did not utilize an optimized stent reconstruction kernel for PCD, the latter potentially further improving in-stent lumen visualization.

The purposes of this study were to investigate qualitative and quantitative CT imaging characteristics of coronary artery stents using a PCD-equipped CT scanner with a dedicated sharp convolution kernel and to test to which extent potential increases in image noise, which can be expected when using sharp image reconstruction filters, can be compensated by iterative image reconstructions (IRs).

MATERIALS AND METHODS

Phantom Setup

For this in vitro study, a phantom simulating stents positioned in coronary arteries and surrounded by epicardial fat was prepared. Eighteen different coronary artery stents from different vendors and made of different materials were included (see Table, Supplemental Digital Content 1, http://links.lww.com/RLI/A384, which lists coronary stent characteristics). Of 18 stents, 16 (88%) were made of stainless surgical steel (316 L), 3 of which (17%) were combined with an additional tantalum coating, 2 (11%) with carbon coating and platinum markers, and 2 (11%) with gold coating. Of 18 stents, 1 (6%) was made of a cobalt chrome alloy and 1 (6%) was composed of a cobalt alloy with titanium coating. Each stent was expanded in a plastic tube with an inner diameter of 3 mm. Plastic tubes had a wall thickness equal to or less than 0.3 mm and a density similar to that of a vessel wall (CT attenuation of 35 Hounsfield Units [HU]). Each tube was filled with iodine contrast agent (Accupaque 350, 350 mg/mL; GE Healthcare, Chicago, IL) diluted to a density of 250 HU at 120 kVp and sealed at both ends. The tubes were embedded in a plastic container (28 × 18 × 12 cm) filled with low-viscosity engine oil simulating epicardial fat. To meet typical fat CT attenuation, oil was calibrated to a value of −100 HU at 120 kVp by adding contrast medium (Lipiodol Ultrafluid, Guerbet, Cedex, France). The phantom was then positioned in the gantry's isocenter and scanned in an orientation of 0° and 90° relative to the scanner's *z*-axis.

CT Data Acquisition and Image Reconstruction

Images were acquired on a modified second-generation 128-slice dual-source CT scanner (SOMATOM Definition Flash, Siemens Healthcare, Erlangen, Germany), which was equipped with 1 conventional EID and 1 CdTe-based PCD. The PCD subsystem of the scanner had 48 × 0.25 slices. Image data were acquired using the PCD at the highest possible resolution ("SHARP" mode), resulting in an effective pixel size in the isocenter of 0.25 × 0.25 mm^2 and a pixel pitch (at the detector) of

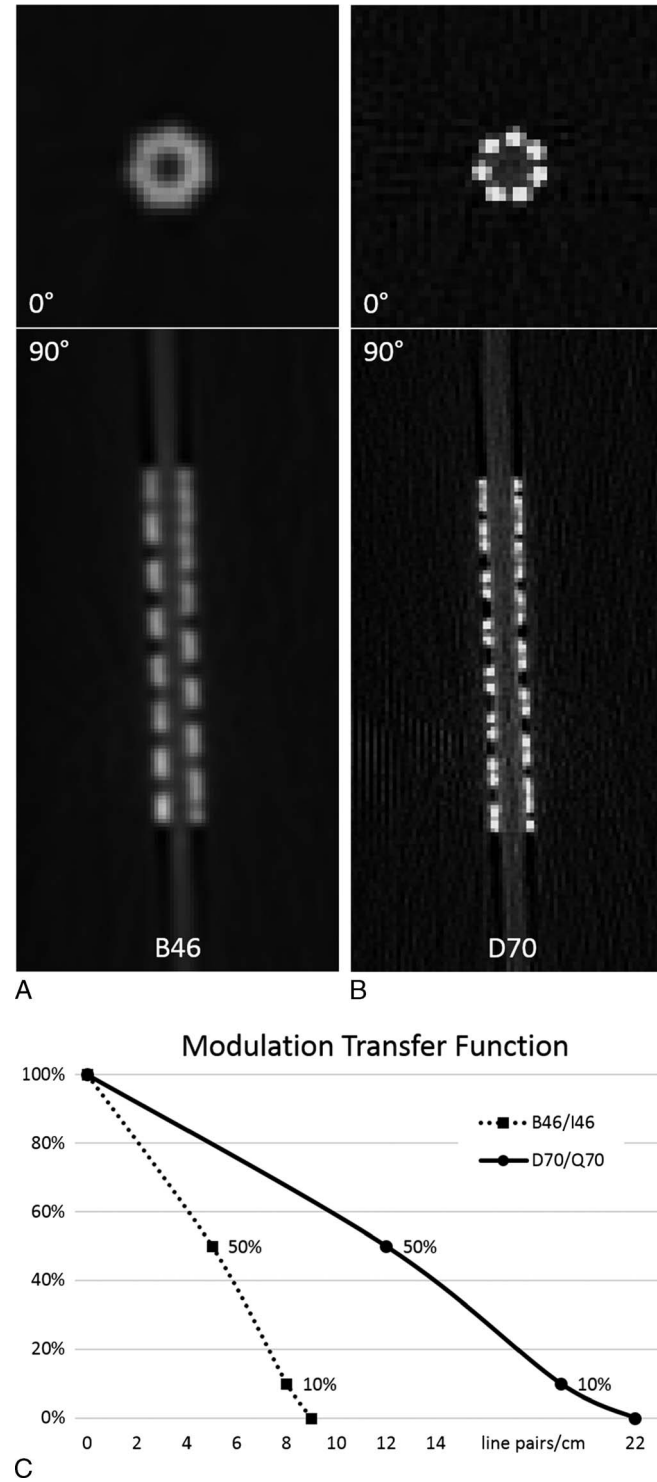

FIGURE 1. Coronary stent phantom reconstructions. Reconstructions of 1 exemplary stent (NIR Royal, Boston Scientific) applying the conventional kernel (A) and a dedicated sharp kernel (B) in combination with FBP are demonstrated. Scans acquired at an orientation of 0° and 90° relative to the scanner's *z*-axis are shown. Note that images in (A) and (B) are reconstructed from the same raw data. In (C), the characteristic MTF values of both kernels are illustrated.

0.45 mm in each dimension. The capability of the PCD to discern x-ray photons at different energy levels was not used, but the entire spectrum was acquired. Image data were obtained using a fixed tube voltage of 100 kVp and a fixed tube current-time product of 100 mAs. These dose settings were chosen similar to the standard protocol for CT stent imaging used in our department. No automatic tube voltage or tube current modulation was used to minimize confounding factors during image comparison. Raw data were reconstructed using the following parameters: slice thickness, 0.6 mm; increment, 0.3 mm; field of view, 150 × 150 mm^2; and image matrix, 512 × 512.

For each stent, the same raw data were reconstructed using a standard convolution kernel and a novel sharp kernel (Fig. 1), both in combination with filtered back-projection (FBP) and IR at different strength levels. Accordingly, the following image data were reconstructed (for information on naming conventions of CT convolution kernels, please see "Discussion"):

First, the reference kernel B46 being a typical kernel for coronary stent imaging in combination with FBP (B46);

Second, the same kernel in combination with sinogram-affirmed IR (SAFIRE) at a strength level of 3 ($I46_3$);

- Third, a dedicated sharp convolution kernel optimized to the technical characteristics of the PCD prototype in combination with FBP (D70);
- Fourth, the dedicated sharp convolution kernel in combination with SAFIRE at a strength level of 3 ($Q70_3$); and
- Fifth, the dedicated sharp convolution kernel in combination with SAFIRE at a strength level of 5 ($Q70_5$).

The image modulation transfer functions (MTFs) of both the conventional and the sharp kernel are illustrated in Figure 1C (for an introduction to this topic and its terminology, please refer to Boreman[18]). For the conventional B46 and $I46_3$ kernels, the characteristic values of the image MTF were ρ_{50} = 5 lp/cm, ρ_{10} = 8 lp/cm, and ρ_2 = 9 lp/cm. Thus, ρ_{50}, ρ_{10}, and ρ_2 were the frequencies for which the MTF value dropped to 50%, 10%, and 0% of its value at ρ = 0 lp/cm, respectively. For the novel D70, $Q70_3$, and $Q70_5$ kernels, characteristic MTF values were ρ_{50} = 12 lp/cm, ρ_{10} = 19 lp/cm, and ρ_2 = 22 lp/cm. To further optimize these kernels for the task of coronary stent imaging, they were designed to accurately delineate contrast edges in the reconstructed image without producing overshoots or undershoots.

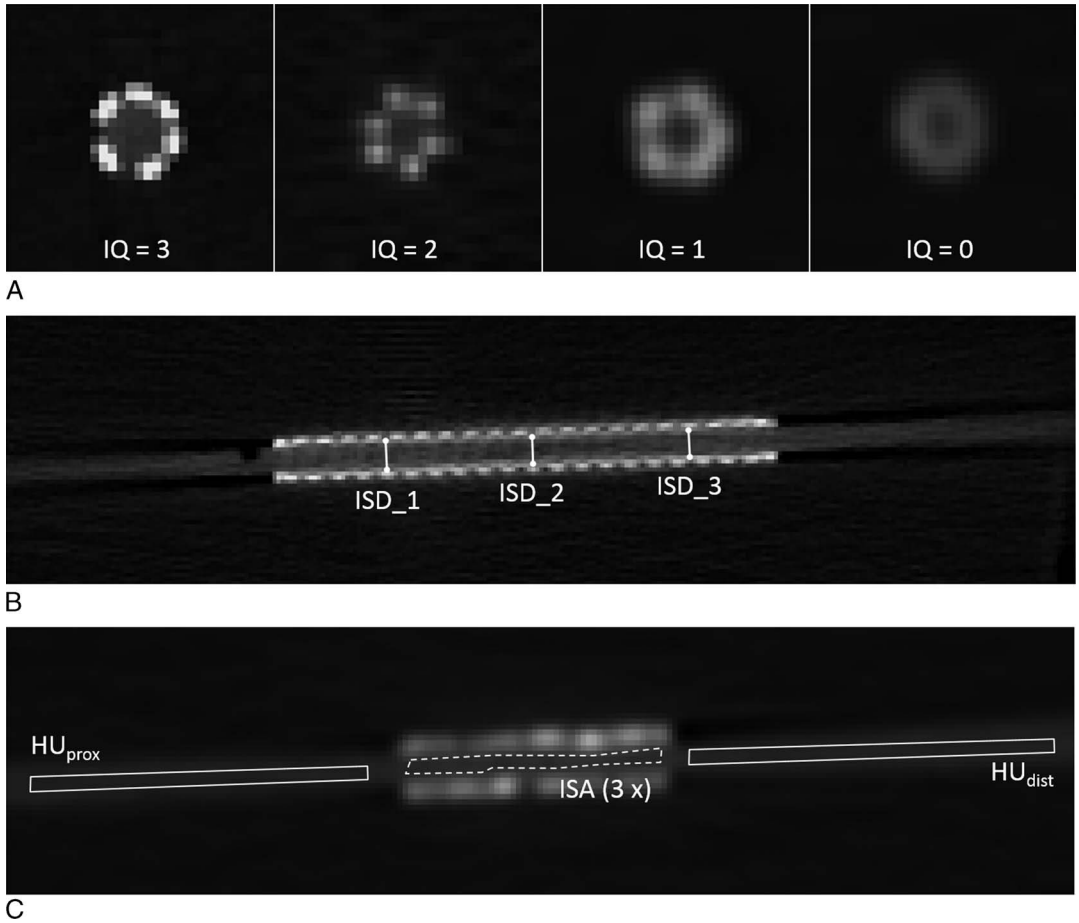

FIGURE 2. Assessment of imaging parameters. An example of different image quality ratings is shown (A; from left to right: Palmaz, Cordis, $Q70_5$, 0°; Sonic Bx, Cordis, D70, 90° MPR; MSM Coronary, Micro Science Medical, B46, 0°; Pura AL 16, Devon Medical, B46, 0°). Before readout, both readers agreed upon the following set of characteristics for image quality scoring: Likert scale 3 = excellent: lumen clearly visible, high strut contrast, gap between struts clearly discernible; 2 = good: lumen visible, medium strut contrast, medium strut gap; 1 = moderate: lumen visibility impaired, medium strut contrast, struts not clearly discriminated; and 0 = insufficient image quality: lumen visibility impaired, low strut contrast, struts not discriminated (A). ISD differences between the measured and true ISD were calculated by averaging 3 manual measurements and subtracting the result from the true diameter (B; Magic Wallstent, Boston Scientific, $Q70_3$, 90°). ISA differences were calculated by subtracting the intraluminal attenuation proximal and distal to the stent from the ISA (C; average from 3 measurements; ZoMaxx, Abbott Vascular Devices, B46, 90°).

Iterative image reconstruction was used to compensate for additional image noise inherently implied by the novel sharp convolution kernel. SAFIRE strength level 3 was applied for both reconstruction kernels, whereas strength level 5 was applied for the sharp kernel only.

Image Analysis

All image data sets (ie, B46, $I46_3$, D70, $Q70_3$, and $Q70_5$) were analyzed by 2 independent, blinded readers (R1 and R2, with 6 and 4 years of experience in cardiovascular imaging, respectively) after 1 conjoint training session. For determining intrareader reliability, reader R2 analyzed all data a second time after 3 weeks for avoiding recall bias.

Qualitative and quantitative analyses were performed using open-source software (ImageJ, US National Institutes of Health, Bethesda, MD) with a fixed window/level setting of 3800/1500 HU. For presenting stent data sets in a random order to the readers, a custom MATLAB script was used (MATLAB; The MathWorks, Natick, MA). Different qualitative and quantitative measures were used for evaluating imaging characteristics, as explained in the following.

The overall image quality of different reconstructions was rated on a subjective 4-point Likert scale (3 = excellent, 2 = good, 1 = moderate, and 0 = insufficient image quality). The following aspects were taken into account for overall image quality rating: lumen visibility, discrimination of struts, and discernibility of gaps between struts. An example of image quality scores is given in Figure 2A. Image quality rating was performed on axial stent images acquired at an angle of 0° and on axial multiplanar reformations (MPRs) of stent images scanned at an angle of 90° relative to the scanner's *z*-axis (Figs. 3 and 4).

The in-stent diameter (ISD) difference was defined as the discrepancy between measured and true ISD (which should equal 0 in the ideal case). The ISD difference was calculated as follows: ΔISD := |(inner diameter of plastic tube − 2*strut thickness) − average measured ISD|. The inner diameter of plastic tubes was 3 mm. The strut thickness was given by the specification of the coronary stents. The ISD was manually measured applying a caliper tool of the analysis software. Three measurements on 90° images were averaged to account for varying stent strut positions and measuring faults as illustrated in Figure 2B.

The in-stent attenuation (ISA) difference was defined as the discrepancy between attenuation values inside the stent lumen and attenuation values measured in the plastic tube outside the stent (which should be 0 in the ideal case). The ISA difference was calculated as follows: ΔISA := average in-stent CT number − average CT number outside the stent. In-stent CT numbers were obtained by use of polygonal regions of interest (ROI) on 90° images (average of 3 measurements). The ROIs were chosen as large as possible, while avoiding inclusion of stent struts and blooming artifacts. Computed tomography numbers outside the stent were obtained by averaging CT numbers of the lumen proximal and distal to the stent as illustrated in Figure 2C.

To obtain an objective measure for image sharpness, intensity profiles of lines through the stent lumen were analyzed (line width = 2 voxels), as previously shown[19] and as illustrated in Figure 5. Negative values of the intensity curve outside the stent were set to 0 to avoid noise influencing the measurement. The maximum steepness of the intensity curve (ie, the maximum absolute derivative) was used as a parameter determining image sharpness: image sharpness := $\max(|[s(x+\varepsilon)-s(x)]/\varepsilon|)$ with $s(x)$ being the signal intensity at point x and $\varepsilon > 0$ (equaling 1 in the discrete case). Three measurements on 0° images were averaged.

Image noise was defined as the standard deviation of CT numbers in an ROI placed in the oil adjacent to the stents (fixed ROI size of 50 × 15 mm^2 = 7.5 cm^2).

Statistical Analysis

Ordinal and continuous variables were expressed as mean ± standard deviation. Interreader and intrareader agreement for the ordinal parameter (ie, image quality) was calculated using Goodman and Kruskal's γ. Interreader and intrareader agreements of continuous imaging parameters (ie, ΔISD, ΔISA, image sharpness, and noise) were evaluated using intraclass correlation coefficients (ICC). According to Landis and Koch, values of 0.61 to 0.8 were interpreted as substantial, and 0.81 to 1.0 as excellent agreement.[20]

Mean differences of the qualitative imaging parameter were tested using a Wilcoxon signed-rank test; mean differences of quantitative imaging parameters were tested using a paired-sample *t* test. A 2-tailed P value < 0.05 was considered to indicate statistical significance. To account for multiple comparisons, Bonferroni correction

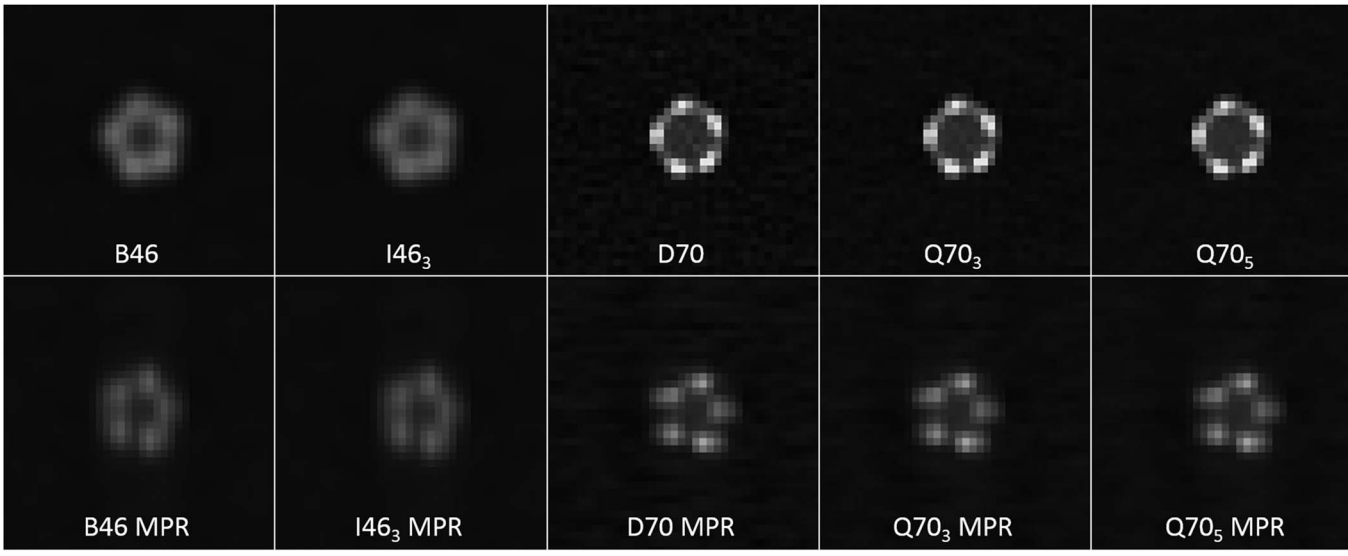

FIGURE 3. Different reconstructions of CT raw data. Ten different reconstructions are illustrated: conventional kernel with FBP (B46) and iterative reconstruction at SAFIRE level 3 ($I46_3$), dedicated sharp convolution kernel with FBP (D70), iterative reconstruction at SAFIRE level 3 ($Q70_3$) and level 5 ($Q70_5$). In the bottom row, axial reformations of the same stent scanned at an angle of 90° relative to the scanner's *z*-axis are shown. Stent used for this figure: CCSV, Micro Science Medical.

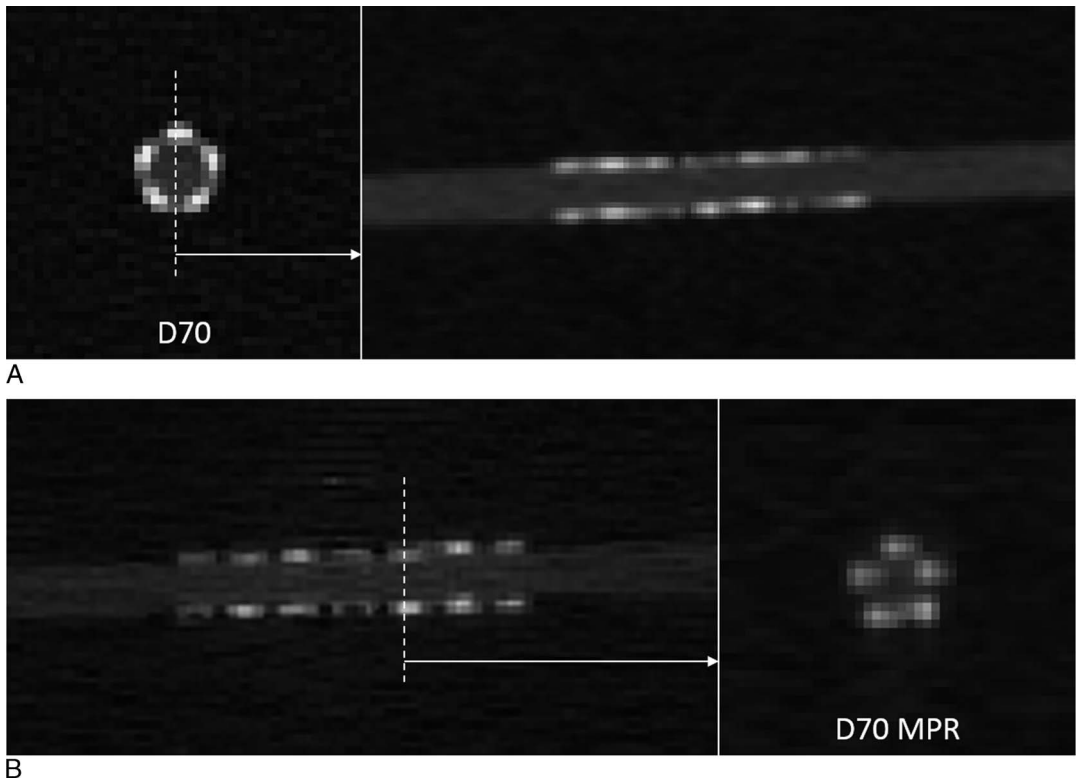

FIGURE 4. Stent image acquisition and reformation. All stents were scanned in an orientation of 0° and 90° relative to the scanner's *z*-axis. On the top (A), the 0° image and its multiplanar reformation (MPR) in a longitudinal stent geometry is shown. On the bottom (B), the 90° image and its axial MPR is shown. Images were reconstructed using the dedicated sharp convolution kernel with FBP (D70). The same stent as in Figure 3 was used for comparison.

was applied, resulting in an adjusted significance level of $P < 0.01$. Statistical analyses were carried out using commercial software (SPSS, IBM, Chicago, IL).

RESULTS

Interreader and Intrareader Agreement

Interreader agreement was excellent for all parameters (γ for image quality = 0.953, ICC = 0.891, 0.968, 0.976, and 0.999 for ΔISD, ISA, image sharpness, and noise, respectively). Intrareader agreement was also excellent for all parameters (γ for image quality = 0.996, ICC = 0.918, 0.988, 0.987, and 0.999 for ΔISD, ΔISA, image sharpness, and noise, respectively).

Image Quality Parameters

Figure 3 shows exemplary images of 1 stent reconstructed with 2 different convolution kernels and different reconstruction methods. Figure 6 and Table 1 show results from the qualitative and quantitative readout.

Regarding overall image quality, all reconstructions using the dedicated sharp convolution kernel (ie, D70, $Q70_3$, $Q70_5$, and their MPRs) yielded significantly better results than the standard kernel reconstructions (ie, B46, $I46_3$, and their MPRs, $P \leq 0.001$ for all comparisons). Comparing data acquired in an orientation of 0° and 90° relative to the scanner's *z*-axis, the image quality of sharp kernel reconstructions was rated significantly higher for 0° than for 90° acquisitions ($P \leq 0.001$ for comparisons D70 vs D70 MPR, $Q70_3$ vs $Q70_3$ MPR, and $Q70_5$ vs $Q70_5$ MPR). For standard kernel reconstructions, there was no significant difference between 0° and 90° acquisitions $P = 0.102$ for comparison B46 vs B46 MPR and $P = 0.096$ for $I46_3$ vs $I46_3$ MPR).

Regarding ISD difference, measurements on images reconstructed with the dedicated sharp convolution kernel were significantly different from measurements on standard kernel images ($P < 0.001$ for all comparisons). Lower ISD differences were observed for all sharp kernel reconstructions.

No significant difference was found between ISA difference measurements on standard kernel images and images reconstructed with the dedicated sharp kernel. The only significant difference was found between D70 and $Q70_3$ image reconstructions (mean ΔISA = 158 and 180, respectively; $P = 0.001$).

In regard to objective image sharpness, all reconstructions based on the dedicated sharp convolution kernel (ie, D70, $Q70_3$, and $Q70_5$) yielded significantly better results than standard kernel reconstructions (ie, B46 and $I46_3$; $P < 0.001$ for all comparisons). Image sharpness in $I46_3$ images was significantly lower than that in corresponding B46 images ($P < 0.001$).

All reconstructions applying the dedicated sharp convolution kernel were associated with significantly higher image noise (all $P < 0.001$, cf. Fig. 7). Combining the sharp kernel with iterative image reconstruction, an average 41% reduction in noise was achieved with SAFIRE 3 ($P < 0.001$ for comparison $Q70_3$ vs D70) and an average 59% reduction in noise for SAFIRE 5 ($P < 0.001$ for comparison $Q70_5$ vs D70).

DISCUSSION

Coronary artery stent lumen visualization with state-of-the-art EID technology is possible with good quality[21] but still needs further improvement. A recent in vitro study investigated whether and how theoretical advantages of PCD technology translate into better coronary stent imaging.[17] This study, however, did not use dedicated sharp

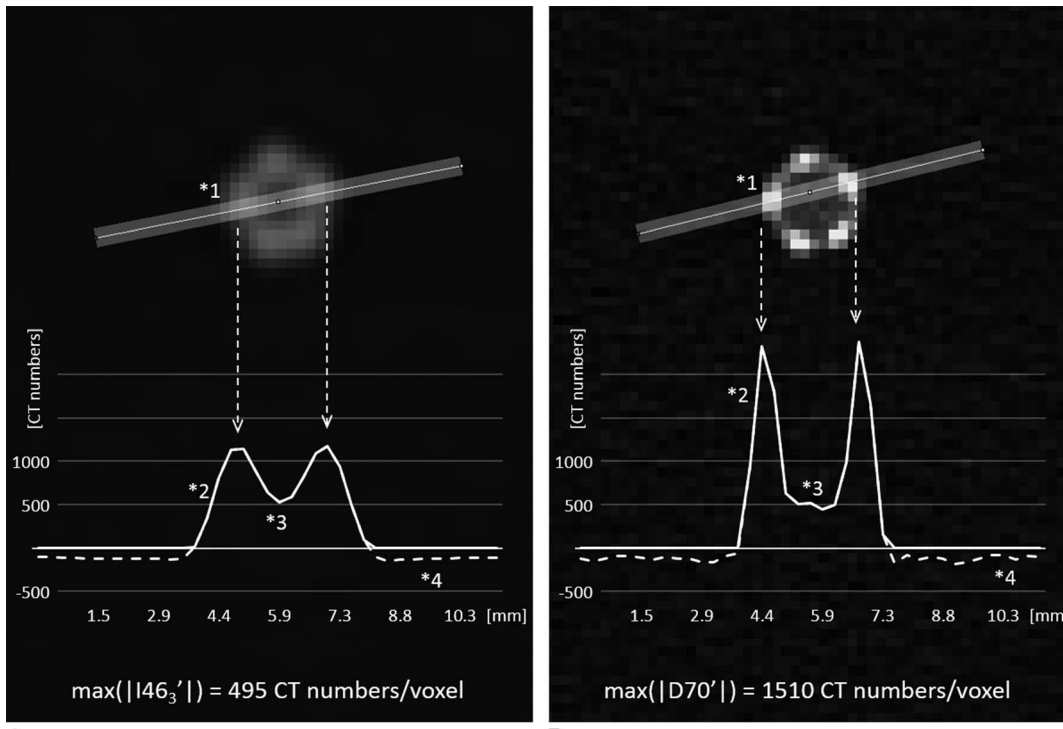

FIGURE 5. Definition of image sharpness. To obtain an objective measure for image sharpness, the intensity profile of a line through the stent lumen (line width = 2 voxels) was analyzed for each stent reconstruction (I46$_3$ and D70 reconstruction of stent CCSV by Micro Science Medical exemplarily shown in (A) and (B), respectively). Lines crossing struts with high signal intensities on both sides of the stent were chosen (*1). Negative values outside the stent (dotted lines) were set to zero (straight lines) to avoid noise influencing the measurement. The maximum absolute derivative was used as an objective parameter describing image sharpness. When comparing the sharp kernel D70 (B) to the conventional kernel I46$_3$ (A), better image quality directly translates into higher steepness of the intensity curve (*2) and broader in-stent lumina (*3). However, also noise outside the stent is higher (*4).

convolution kernels, which have the potential for a better exploitation of the potential of the PCD array set-up.

Our study adds to the literature by using and testing a dedicated sharp convolution kernel adapted to the intrinsic higher spatial resolution of the PCD array for coronary stent imaging. We found that PCD image reconstructions applying this dedicated sharp convolution kernel significantly improved the overall image quality, reduced ISD differences, and increased image sharpness (mathematically calculated by analyzing intensity profiles through the stent) as compared with a standard kernel but came along with a higher noise level. This increase in image noise can be considerably reduced when using iterative image reconstruction.

For our study, we tried to include a well-balanced selection of different types of CT convolution kernels. B46 and I46$_3$ immediately come to mind for CT stent imaging in today's clinical routine, because they were specifically designed for this purpose. D70 and Q70$_3$ were included as dedicated sharp kernels to be tested in this study. Q70$_5$ was included to test for maximum noise reduction by means of higher-strength-level IR. In general, the following naming conventions are used for CT convolution kernels: *B kernels* are standard reconstruction kernels with FBP. These kernels are designed for specific imaging tasks in the various body regions. Therefore, these kernels are available in different sharpness levels: the higher the number in the second place, the higher is the image sharpness. The number in the third place encodes the image properties beyond sharpness, for example, the *Bx6* kernels are designed for imaging the heart region. *I kernels* are the iterative counterparts of the B kernels. Besides applying iterative image reconstruction, all properties of the I kernels are identical to those of the corresponding B kernels. *D kernels* are FBP kernels designed to provide images with quantitative HU values. "Quantitative" in this context means that the kernels do not alter the impression of contrast edges in the image, that is, those kernels do not produce overshoots or undershoots at contrast edges. *Q kernels* are the iterative counterparts of D kernels. Iterative reconstruction is switched on for these kernels, whereas all other imaging properties remain identical to the corresponding D kernels. Both the D and Q kernels are designed in a way that they transfer the maximal spatial frequency of the imaging system into the reconstructed image.

The novel kernels D70, Q70$_3$, and Q70$_5$ used in the present study were specifically designed for stent imaging on the high-resolution PCD system. Characteristic values of the image MTF were optimized. The resulting image sharpness (determined by ρ_2 values of the image MTF) in the D70/Q70 images was significantly increased by a factor of 2 to 3 compared with B46/I46$_3$ images. Furthermore, the dedicated sharp kernels were designed to accurately depict contrast edges in the CT images, yielding exact separation of soft tissue/stent borderlines and resulting in a significant 33% to 38% decrease in the discrepancy between measured and true ISD (ie, ISD difference). This finding is highly important for coronary stent imaging because an accurate depiction of soft tissue/stent borderlines is necessary for clinical in-stent lumen evaluation.

Comparing ISA to CT numbers measured outside the stent (ie, ISA difference), we found that values did not differ significantly between the conventional and dedicated kernels—meaning that the increase in CT numbers inside the stent lumen was comparable for both kernels. It follows that the sharp kernel does not offer definite advantages over the standard kernel regarding this aspect. Instead, ISA values seem to be mainly determined by the raw data itself. This

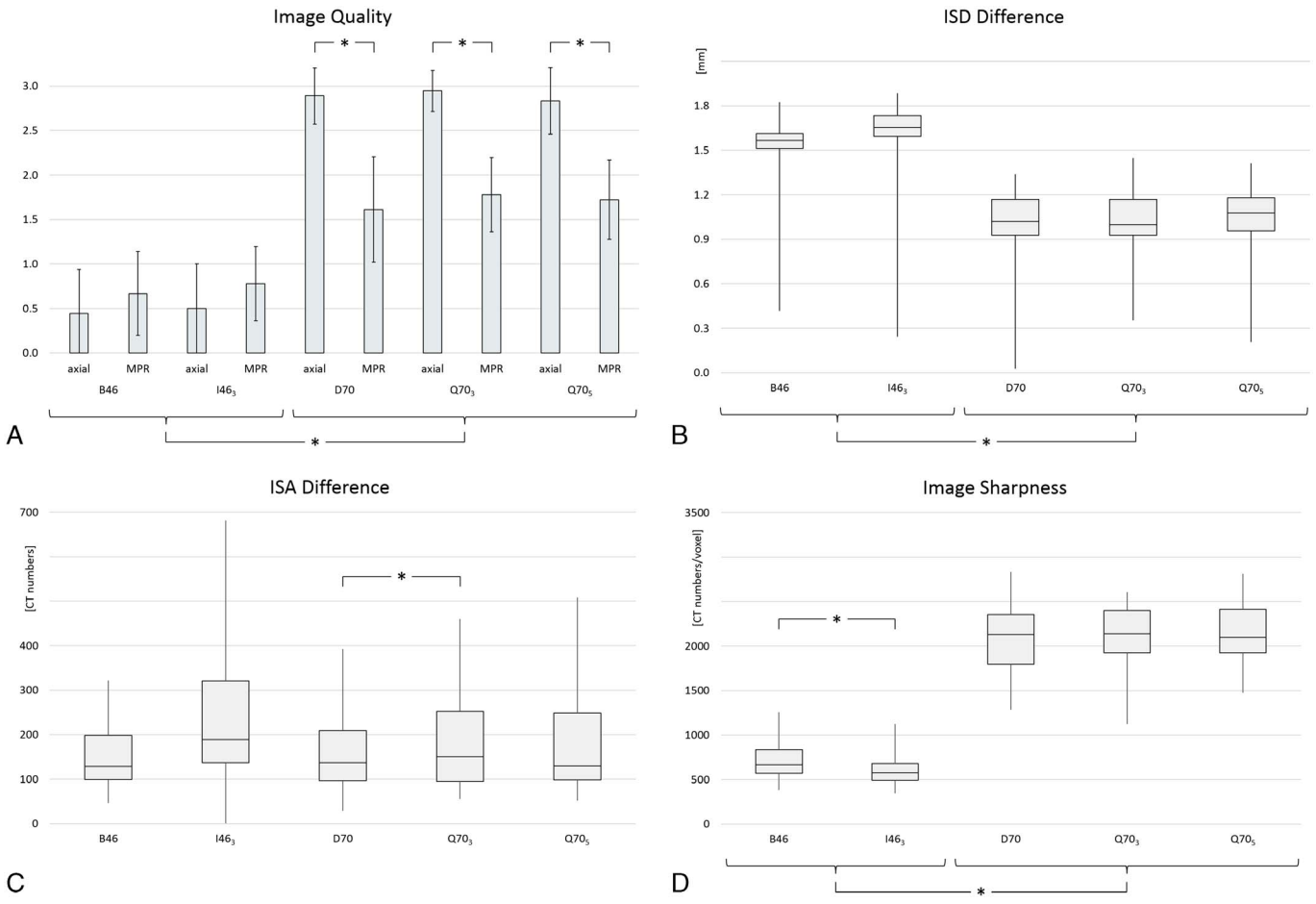

FIGURE 6. Results from image analysis. Bar chart of overall image quality (A) and boxplots of ISD difference (B), ISA difference (C), and image sharpness (D).

possible explanation is supported by findings from Mannil et al[17] that ISA differences were significantly lower for PCD images when compared with EID.

Comparing the results of 0° and 90° phantom positioning relative to the scanner's *z*-axis, we surprisingly found that 90° MPRs of conventional kernel reconstructions showed a tendency toward higher image quality ratings compared with their 0° counterparts (without reaching the level of significance, $P = 0.102$ for comparison B46 vs B46 MPR and $P = 0.096$ for I46$_3$ vs I46$_3$ MPR). In contrast, for reconstructions applying the novel sharp kernel, we found that 90° images showed a significantly lower image quality than their 0° counterparts. However, these 90° sharp kernel images still offered significantly higher image quality compared with 0° and 90° images reconstructed with the standard kernel. Therefore, the

TABLE 1. Results From Qualitative and Quantitative Image Analysis

	Image Quality					
	0°	90°	ISD Difference, mm	ISA Difference (CT Numbers)	Image Sharpness (CT Numbers/Voxel)	Noise (CT Numbers)
B46	0.4 ± 0.5	0.7 ± 0.5	1.5 ± 0.3	151 ± 76	728 ± 246	16 ± 1
I46$_3$	0.5 ± 0.5	0.8 ± 0.4	1.6 ± 0.3	202 ± 154	632 ± 229	16 ± 1
D70	2.9 ± 0.3	1.6 ± 0.6	1.0 ± 0.3	158 ± 92	2069 ± 411	111 ± 3
Q70$_3$	2.9 ± 0.2	1.8 ± 0.4	1.0 ± 0.2	180 ± 107	2070 ± 419	65 ± 2
Q70$_5$	2.8 ± 0.4	1.7 ± 0.4	1.0 ± 0.2	179 ± 114	2147 ± 366	46 ± 2

0° = image data acquired with an orientation of 0° relative to the scanner's *z*-axis; 90° = image data acquired with an orientation of 90° relative to the scanner's *z*-axis; B46 = standard kernel combined with filtered back-projection; I46$_3$ = standard kernel with iterative reconstruction at strength level 3; D70 = novel sharp kernel with filtered back-projection; Q70$_3$ = novel sharp kernel with iterative reconstruction at strength level 3; Q70$_5$ = novel sharp kernel with iterative reconstruction at strength level 5. Ordinal and continuous variables are expressed as mean ± SD.

ISD indicates in-stent diameter; ISA, in-stent attenuation; CT, computed tomography.

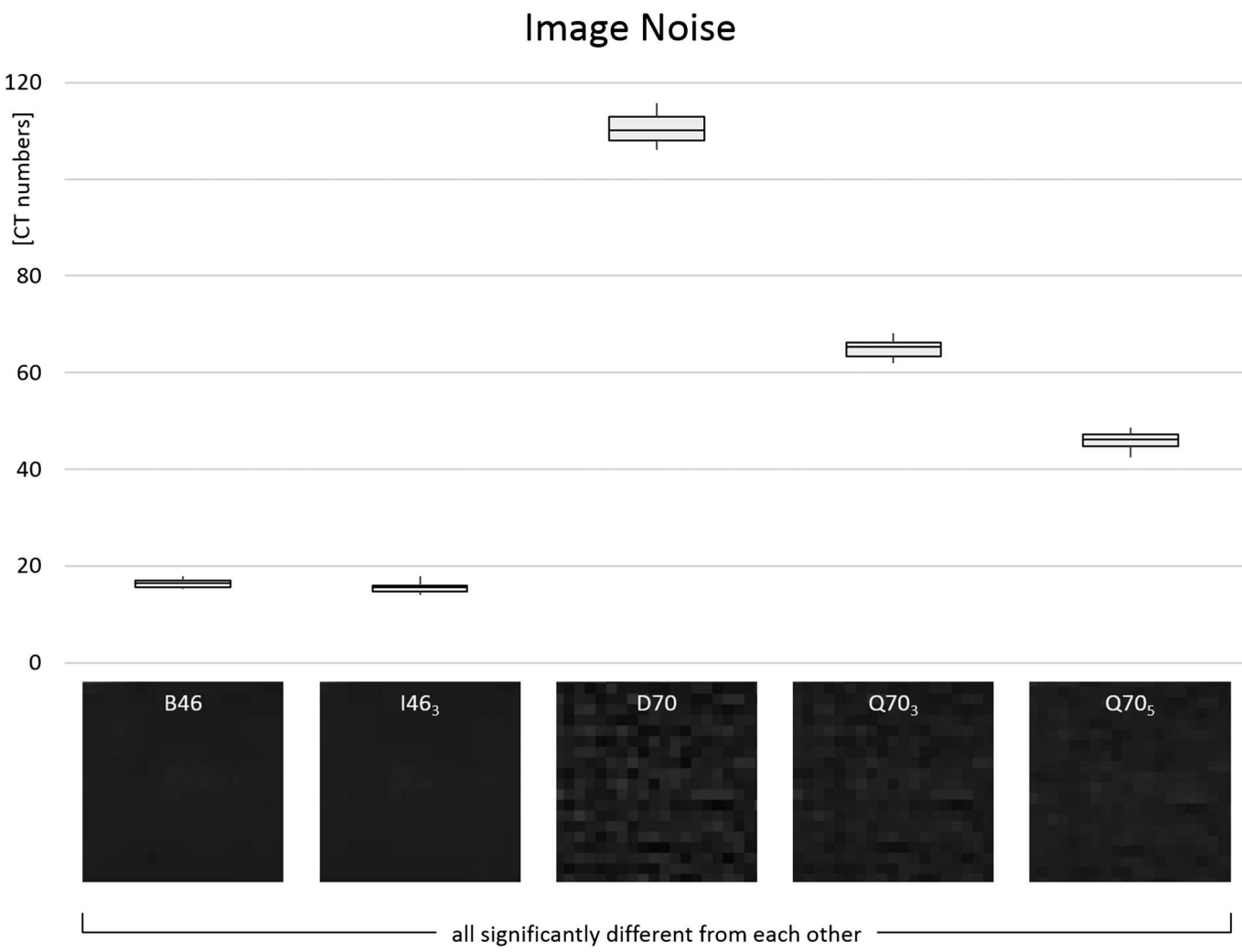

FIGURE 7. Image noise of different reconstructions. Reconstructions of the same CT raw data with the dedicated sharp convolution kernel D70 led to significantly higher image noise as compared to the conventional kernel B46. Noise increase could partly be suppressed by application of iterative reconstruction at SAFIRE level 3 and 5 (ie, $Q70_3$ and $Q70_5$, respectively). Below the boxplot, examples of noise in the oil adjacent to 1 arbitrary stent are shown.

novel technique might be an important step improving imaging characteristics not only in-plane but also in through-plane direction.

First in vivo measurements found that PCD technology, in combination with standard convolution kernels, can yield lower image noise and an increased contrast-to-noise ratio in low-dose chest CT[16] and low-dose lung cancer screening.[15] In contrast, noise measurements in our study showed that use of dedicated sharp convolution kernels was associated with a significant increase in image noise compared with standard kernels. The increase in noise is caused by the fact that FBP is a linear reconstruction algorithm for which boosted sharpness always comes at the cost of additional image noise. By applying IR instead of FBP, we could show that the increase in image noise could be reduced in part. However, even when applying IR, image noise was still higher in the sharp kernel reconstructions. This finding indicates that a tradeoff between image sharpness and noise must also be found for PCD-equipped CT.

For IR, we applied SAFIRE level 3 because this strength level is commonly used in clinical routine.[22,23] In addition, we included SAFIRE level 5 to our analysis, despite of its known "plastic-like," blotchy image appearance.[24] By doing so, we wanted to evaluate to which extent noise can be maximally reduced. Furthermore, recently introduced IR algorithms are known to reduce the unfavorable image texture also at higher strength levels.[24]

Because PCD arrays translate individual photons into a proportional electric current, the technology inherently offers spectral information on the incoming flux of x-ray photons. In the context of vascular and stent imaging, this capacity was found to offer various benefits. Using specific contrast agents in an animal model, spectral CT could provide information about atherosclerotic plaque composition.[11] Using the characteristic k-edge of gadolinium, spectral CT showed the potential to differentiate among intravascular gadolinium-based contrast agent, calcified plaque, and stent material,[12] possibly improving intraluminal depiction for the diagnostics of in-stent restenosis. First in vivo results of vascular imaging of the head and neck showed significantly higher image quality, lower image noise, and less artifacts[25] for a spectral PCD scanner compared with single-energy CT scans using a conventional EID. Using the spectral information, virtual monoenergetic images as well as iodine maps could be calculated, with the latter showing significantly higher contrast-to-noise ratios compared with nonspectral PCD.[25] Regarding cardiac imaging, the possibility to combine spectral PCD with dual contrast was demonstrated in a recent proof-of-principle study.[13] By applying gadolinium as well as iodinated

contrast agents and taking advantage of the spectral capabilities of the PCD, myocardial first-pass and late enhancement could be assessed simultaneously.[13] In our study, the spectral capabilities of the PCD were not evaluated. By intentionally setting the energy threshold to a fixed value of 25 keV, our PCD images were acquired with the entire x-ray energy spectrum. This was done because in formalized in vitro measurements, all aspects of the new PCD technology should be evaluated separately from each other. By assessing the advances of dedicated reconstruction kernels in an isolated fashion, we could show its impact on PCD image reconstruction without further confounding factors possibly diluting the results and the data-driven conclusion. However, future research also needs to evaluate the impact of different energy settings on PCD stent imaging.

We must acknowledge the following study limitations. First, this was an in vitro study with inherent limitations. However, a well-established phantom setup verified in many previous studies was used.[4,17,21,26] Second, a relatively low number of coronary stents was included, necessitating larger sample sizes to confirm our results. However, we found stable results for all measured parameters, and subjective differences in image quality were quite impressive. We therefore believe that our findings will hold true also for other, larger studies performed in the future. Third, we did not simulate presence of in-stent restenosis in our coronary stent phantom. However, we assume that better image quality and better in-stent delineation would also translate into superior in-stent restenosis evaluation.

In conclusion, our in vitro study indicates considerably improved imaging characteristics of PCD technology when used with dedicated sharp convolution kernels for coronary in-stent lumen visualization, representing a step forward for tapping the potential of the novel CT detector technology.

REFERENCES

1. De Santis D, Jin KN, Schoepf UJ, et al. Heavily calcified coronary arteries: advanced calcium subtraction improves luminal visualization and diagnostic confidence in dual-energy coronary computed tomography angiography. *Invest Radiol*. 2018;53:103–109.
2. Higashigaito K, Husarik DB, Barthelmes J, et al. Computed tomography angiography of coronary artery bypass grafts: low contrast media volume protocols adapted to tube voltage. *Invest Radiol*. 2016;51:241–248.
3. Schroeder S, Achenbach S, Bengel F, et al. Cardiac computed tomography: indications, applications, limitations, and training requirements: report of a Writing Group deployed by the Working Group Nuclear Cardiology and Cardiac CT of the European Society of Cardiology and the European Council of Nuclear Cardiology. *Eur Heart J*. 2008;29:531–556.
4. Maintz D, Juergens K-U, Wichter T, et al. Imaging of coronary artery stents using multislice computed tomography: in vitro evaluation. *Eur Radiol*. 2003;13:830–835.
5. Gutjahr R, Polster C, Henning A, et al. Dual energy CT kidney stone differentiation in photon counting computed tomography. *Proc SPIE Int Soc Opt Eng*. 2017;10132.
6. Gutjahr R, Halaweish AF, Yu Z, et al. Human imaging with photon counting-based computed tomography at clinical dose levels: contrast-to-noise ratio and cadaver studies. *Invest Radiol*. 2016;51:421–429.
7. Leng S, Zhou W, Yu Z, et al. Spectral performance of a whole-body research photon counting detector CT: quantitative accuracy in derived image sets. *Phys Med Biol*. 2017;62:7216–7232.
8. Yu Z, Leng S, Jorgensen SM, et al. Initial results from a prototype whole-body photon-counting computed tomography system. *Proc SPIE Int Soc Opt Eng*. 2015;9412:94120 W.
9. Leng S, Yu Z, Halaweish A, et al. Dose-efficient ultrahigh-resolution scan mode using a photon counting detector computed tomography system. *J Med Imaging (Bellingham)*. 2016;3:043504.
10. de Vries A, Roessl E, Kneepkens E, et al. Quantitative spectral K-edge imaging in preclinical photon-counting x-ray computed tomography. *Invest Radiol*. 2015;50:297–304.
11. Cormode DP, Roessl E, Thran A, et al. Atherosclerotic plaque composition: analysis with multicolor CT and targeted gold nanoparticles. *Radiology*. 2010;256:774–782.
12. Feuerlein S, Roessl E, Proksa R, et al. Multienergy photon-counting K-edge imaging: potential for improved luminal depiction in vascular imaging. *Radiology*. 2008;249:1010–1016.
13. Symons R, Cork TE, Lakshmanan MN, et al. Dual-contrast agent photon-counting computed tomography of the heart: initial experience. *Int J Cardiovasc Imaging*. 2017;33:1253–1261.
14. Leng S, Gutjahr R, Ferrero A, et al. Ultra-high spatial resolution, multi-energy CT using photon counting detector technology. *Proc SPIE Int Soc Opt Eng*. 2017;10132.
15. Symons R, Cork TE, Sahbaee P, et al. Low-dose lung cancer screening with photon-counting CT: a feasibility study. *Phys Med Biol*. 2017;62:202–213.
16. Symons R, Pourmorteza A, Sandfort V, et al. Feasibility of dose-reduced chest CT with photon-counting detectors: initial results in humans. *Radiology*. 2017;285:980–989.
17. Mannil M, Hickethier T, von Spiczak J, et al. Photon-counting CT: high-resolution imaging of coronary stents. *Invest Radiol*. 2018;53:143–149.
18. Boreman GD. *Modulation Transfer Function in Optical and Electro-Optical Systems*. Bellingham, WA: SPIE Press; 2001.
19. von Spiczak J, Morsbach F, Winklhofer S, et al. Coronary artery stent imaging with CT using an integrated electronics detector and iterative reconstructions: first in vitro experience. *J Cardiovasc Comput Tomogr*. 2013;7:215–222.
20. Landis JR, Koch GG. The measurement of observer agreement for categorical data. *Biometrics*. 1977;33:159–174.
21. Gassenmaier T, Petri N, Allmendinger T, et al. Next generation coronary CT angiography: in vitro evaluation of 27 coronary stents. *Eur Radiol*. 2014;24:2953–2961.
22. Hardie AD, Nelson RM, Egbert R, et al. What is the preferred strength setting of the sinogram-affirmed iterative reconstruction algorithm in abdominal CT imaging? *Radiol Phys Technol*. 2015;8:60–63.
23. Kim SH, Yoon JH, Lee JH, et al. Low-dose CT for patients with clinically suspected acute appendicitis: optimal strength of sinogram affirmed iterative reconstruction for image quality and diagnostic performance. *Acta Radiol*. 2015;56:899–907.
24. Morsbach F, Desbiolles L, Raupach R, et al. Noise texture deviation: a measure for quantifying artifacts in computed tomography images with iterative reconstructions. *Invest Radiol*. 2017;52:87–94.
25. Symons R, Reich DS, Bagheri M, et al. Photon-counting computed tomography for vascular imaging of the head and neck: first in vivo human results. *Invest Radiol*. 2018;53:135–142.
26. Hickethier T, Baeßler B, Kroeger JR, et al. Monoenergetic reconstructions for imaging of coronary artery stents using spectral detector CT: in-vitro experience and comparison to conventional images. *J Cardiovasc Comput Tomogr*. 2017;11:33–39.